PAPER • **OPEN ACCESS**

Isolation by dialysis and characterization of luminescent oxidized carbon nanoparticles from graphene oxide dispersions: a facile novel route towards a more controlled and homogeneous substrate with a wider applicability*

To cite this article: Francesco Amato *et al* 2025 *Nanotechnology* **36** 185602

OPEN ACCESS
IOP Publishing
Nanotechnology

Nanotechnology **36** (2025) 185602 (12pp) https://doi.org/10.1088/1361-6528/adc608

Isolation by dialysis and characterization of luminescent oxidized carbon nanoparticles from graphene oxide dispersions: a facile novel route towards a more controlled and homogeneous substrate with a wider applicability*

Francesco Amato[1,6,], Martina Fazi[1,6], Leonardo Giaccari[1], Sara Colecchia[1], Giordano Perini[2,3], Valentina Palmieri[2,3,4], Massimiliano Papi[2,3], Pietro Altimari[1], Alessandro Motta[1,5], Mauro Giustini[1], Robertino Zanoni[1] and Andrea Giacomo Marrani[1,**]**

[1] Dipartimento di Chimica, Università di Roma La Sapienza, p.le A. Moro 5, I-00185 Rome, Italy
[2] Dipartimento di Neuroscienze, Università Cattolica del Sacro Cuore, Largo Francesco Vito 1, 00168 Rome, Italy
[3] Fondazione Policlinico Universitario 'A. Gemelli' IRCSS, Largo A. Gemelli, 8 00168 Rome, Italy
[4] Istituto dei Sistemi Complessi, CNR, Via dei Taurini 19, 00185 Rome, Italy
[5] Consorzio INSTM UdR Roma 'La Sapienza', p.le A. Moro 5, I-00185 Rome, Italy

E-mail: francesco.amato@uniroma1.it and andrea.marrani@uniroma1.it

Received 16 December 2024, revised 13 March 2025
Accepted for publication 27 March 2025
Published 4 April 2025

Abstract

Graphene Oxide (GO) is a two-dimensional (2D) nanomaterial largely exploited in many fields. Its preparation, usually performed from graphite in an oxidant environment, generally affords 2D layers with a broad size distribution, with overoxidation easily occurring. Here, we investigate the formation, along the Hummers synthesis of GO, of carbon nanoparticles (CNPs) isolated from GO and characterized through morphological and spectroscopic techniques. The purification methodology here applied is based on dialysis and results highly advantageous, since it does not involve chemical processes, which may lead to modifications in the

[6] Authors contributed equally to this work.
* This work is dedicated to Prof. Maurizio Prato, on the occasion of his 71st birthday.
** Authors to whom any correspondence should be addressed.

composition of GO layers. Using a cross-matched characterization approach among different techniques, such as x-ray photoelectron spectroscopy, cyclic voltammetry and fluorescence spectroscopy, we demonstrate that the isolated CNP are constituted by layers that are highly oxidized at the edges and are stacked due to π–π interaction among their aromatic basal planes and H–bonded via their oxidized groups. These results, while representing a step forward in the comprehension of the structure of long-debated carbon debris in GO, strongly point to the introduction of dialysis as an indispensable step toward the preparation of more controlled and homogeneous GO layers and to its use for the valorization of low molecular weight GO species as luminescent CNPs.

Supplementary material for this article is available online

Keywords: graphene oxide, carbon nanoparticles, dialysis, oxidative debris, XPS

1. Introduction

Graphene oxide (GO), the oxidized form of graphene, is a two-dimensional and non-stoichiometric material, prevalently constituted of sp^2 hybridized carbon and oxygen atoms [1, 2]. Its synthesis and remarkable properties have been widely investigated for the variety of physical-chemical, engineering, medical and many other applications [3, 4].

GO is an amphiphilic species owing to the presence of conjugated and aromatic domains coupled to oxygen-based functional groups (OFGs) that ensure water-dispersibility in a wide range of pH [5, 6]. In particular, it is accepted that both hydroxyl and epoxide groups are mainly localized on the basal plane of the C layers, whereas the less abundant carboxylic functionalities are restricted to the edges together with ketone and lactone groups [7–9]. Noteworthy, the biological activity of GO is highly dependent on its surface chemical composition, which affects the interaction with biomacromolecules [10–12].

GO is prepared from graphite through a top-down approach in which oxidant agents bring about an interruption of the extended π-aromatic network with the creation of oxygen-based structural defects, leading to the opening of an electronic energy gap [13, 14]. Types and relative amounts of oxidant, as well as the presence of acidic agents, provide layers of GO with different O/C ratios, with a tailoring of specific functional groups [15–17]. Moreover, the size distribution in terms of average number of layers is also affected by sonication cycles, since they improve the exfoliation efficiency [18, 19].

In the synthesis of GO, graphite powder is quickly eroded by the oxidant agents and the smaller flakes of graphite are presumably oxidized significantly faster compared to the larger ones [20]. As a result, layers of GO are formed with different O/C ratios and lateral size, ranging from tens of nanometers up to few micrometers [21]. In the light of the mechanistic hypotheses, some *overoxidized* fragments could be easily formed during the preparation of GO, as reported by Rourke *et al* [22], who elegantly theorized the presence of oxidative complexes constituted of layers of GO on which highly oxidized fragments are adsorbed, denominated *oxidative debris* (OD). OD have sometimes been represented as small polymers of humic acids, though their structure and physical-chemical properties have been much debated in recent years. [22, 23] Since OD particles are very rich in OFGs, they can compete with the larger layers of GO in the functionalization reactions, affecting their distinctive overall physical-chemical properties. In an attempt to isolate OD from GO dispersions, procedures reported in the literature made use of basic washing, while centrifugation cycles performed after ultrasonication at different times were applied to GO nanoplatelets prepared from graphite nanofibers [24, 25]. In particular, GO dispersions were treated with aqueous solutions of NaOH (either 1 M or 0.01 M, in both cases at reflux for one hour). Subsequently, GO and OD were collected after water removal as black and white powders, respectively [22]. The collected amount of OD was found to be particularly high when both $KMnO_4$ and $NaNO_3$ were used for the synthesis of GO [24], while the type of base employed negligibly affected the OD luminescence properties, as reported by Thomas *et al* [26]. In particular, the darkening of the aqueous dispersion of pristine GO (pGO) was immediately observed either after the addition of a NaOH solution or after a short reflux with ammonia. Subsequently, after centrifugation, the isolated OD and base-washed GO showed distinctive emission properties upon excitation at 400 nm, consisting in a very intense luminescence peaked at 520 nm for the former and no fluorescence for the latter [26], while pGO displays a broad and less intense peak of fluorescence emission at 610 nm [26]. Therefore, the luminescence of pGO is presumably due to the presence of adsorbed OD, that, once removed after basic washing, were identified as organic fragments with molecular weights (MW) $<$1000 Da and rich in molecular fluorophores [26, 27]. The same authors reported in another paper dealing with the synthesis of GO and the stripping of OD, that the morphological characterization by atomic force microscopy (AFM) was not feasible due to the too low dimensions of OD ($\sim$0.5 nm) [28]. On a small scale a hydrothermal treatment with ammonia of GO containing amorphous OD allowed to obtain crystalline, nitrogen-doped, graphene quantum dots with an average height of 1.3 nm [23, 29]. In another work, OD were also stripped from the layers of GO

in the presence of aqueous ammonia (∼6 M) followed by a hydrothermal treatment of the mixture at 100 °C × 1 h followed by a centrifugation step. Then, the OD dispersed in the supernatant were characterized through AFM, whose images displayed isolated species, mostly smaller than 100 nm in lateral size and 1–10 nm in height [23, 30]. Finally, Faria *et al* investigated for the first time the antimicrobial properties of OD with an average height of 1.7 ± 0.3 nm toward *E. coli* by concentrating the supernatant obtained from the centrifugation of an aqueous dispersion of GO treated with NaOH at 80 °C × 1.5 h [23, 31].

Although very effective, the basic washing of GO as a method for isolation of the OD has some severe drawbacks, such as the degradation of the GO [22, 24, 32, 33]. Under strong alkaline conditions, in fact, both GO decarboxylation and disproportionation reactions occur and the corresponding water dispersions become optically darker [34, 35].

It is evident from the above-mentioned results, that both the most correct isolation methodology and the actual structure and chemical composition of the so-called OD are still a matter of debate.

In this work, both these issues have been addressed. In particular, we have investigated both the morphology and the chemical properties of oxidized carbon nanoparticles (CNPs) directly collected from GO aqueous dispersions by dialysis, avoiding the use of any basic washing, therefore eliminating any possible source of degradation or chemical modification of GO. The use of dialysis membranes with different MW cut-offs has allowed us to select different populations of CNPs. Through the proposed method, low MW particles can be easily isolated and purified, and their properties ascertained.

The isolated CNPs could have important potential applications, i.e. gas sensors [36], fluorescent sensing and imaging [37], and solar cells [38].

2. Experimental section/ methods

All reagents and solvents were purchased from Sigma-Aldrich, Fluka, Alfa Aesar, VWR, TCI and used as received. Dialysis membranes with cut-offs of 12–14, 3.5–5 and 1 kDa (Spectra/Por®) were activated using Milli-Q water with a resistivity of 18.2 MΩ × cm at 25 °C.

Pristine GO (pGO) was synthesized by following an already-reported procedure [14, 39, 40].

For the workup, a filter paper filtration was applied and the obtained solid was centrifuged (Fisher Scientific, Sorvall ST1R Plus) in HCl 1.12 M and Milli-Q water (four times) at 4000 rpm for 30 min. During these purification steps, the supernatant was always discharged and replaced with Milli-Q water. The solid was then transferred in a round-bottom flask and resuspended with Milli-Q water; in order to ensure a proper exfoliation, the resulting mixture was stirred for one night. At this point, the dispersion was sonicated in a water bath for 30 min and then centrifuged at 3000 rpm for 40 min in order to separate the graphite oxide still present from the yellowish supernatant. This procedure was repeated until an almost colorless supernatant was obtained. Finally, the dispersion of pGO was freeze-dried and the resulting solid powder was stored in a desiccator.

High and low MW fractions of GO were separated via dialysis of the pGO sample. 0.4 g of freeze-dried pGO were dispersed in 15 ml of Milli-Q water and subsequently transferred into the dialysis membrane of the selected cut-off and left immersed under stirring for a total time of 72 h in 0.6 l Milli-Q water (1:40 v/v ratio). After the first 24 h and then again at interval times of 12 h, the water was replaced. The discharged dialysis waters collected at each time interval were checked by UV–Vis spectroscopy, which resulted in a flat signal after 72 h, also after their concentration under vacuum at 35 °C using a rotavapor, indicating that dialysis was complete due to the absence of nanoparticles. The dialysis waters containing the low MW fractions were collected and concentrated as stated before (dy-w *x* samples, with x = MW cut-off of the membrane used in the dialysis). Finally, the aqueous dispersion of the dialyzed GO (dGO *x* samples, with x = MW cut-off of the membrane used in the dialysis) was freeze-dried and stored in a desiccator.

All the experimental activity henceforth described was conducted at room temperature, in order to avoid any possible chemical reduction effect exerted by heat on the GO materials [41].

AFM Samples for AFM were obtained by drop-casting 100 μl of each sample dispersion (10 μg ml^{-1}) on mica slides, which were left to air-dry overnight. AFM images were acquired with a NanoWizard II (JPK Instruments AG, Berlin, Germany) equipped with cantilevers with high aspect-ratio conical Si tips (CSC36 Mikro-Masch, Tallinn, Estonia), with an end radius of about 10 nm, a half conical angle of 20°, and a spring constant of 0.6 N m^{-1}. The difference between the substrate peak value (set to zero) and the single flake GO peak allowed to determine the average thickness, as previously reported [42], while the lateral size distribution was determined through image analysis (FIJI software) from the square root of the flakes area.

UV–Vis and Raman spectroscopy: UV–Vis spectra were recorded with a Cary 50 UV–Vis spectrophotometer at room temperature using quartz cuvettes with 10 mm path-length. Raman spectra were recorded at room temperature in backscattering geometry with an inVia Renishaw micro-Raman spectrometer equipped with an air-cooled CCD detector and super-Notch filters. An Ar^+ ion laser (λ_{laser} = 514 nm) was used, coupled to a Leica DLML microscope with a 20× objective. The spectra were calibrated using the 520.5 cm^{-1} line of the Si(100) support and the resolution was set to 2 cm^{-1}. Raman spectra were acquired in 6–10 different spots on the surface of the samples with 1% of power, 10 s of spectral acquisition, and 20 scans.

Fluorescence spectroscopy: spectra were recorded using a Horiba Jovin-Yvon spectrofluorometer (Fluoromax 2) at 25 °C (Peltier-thermostated sample holder from Quantum Northwest, Liberty Lake, WA, USA, controlled by the TC1 unit via the T-App software from the same manufacturer); slits: 2.5/2.5 nm; cell: 1.0 × 1.0 cm. All measurements were

performed on aqueous dispersions with an optical density below 0.1 at 300 nm. Fluorescence lifetime measurements were performed with the time correlated single photon counting (TCSPC) technique using an instrument of local design elsewhere described [43, 44]. Measurements details will be given at due time. TCSPC data were fitted to a reconvolution function among the instrument response function and the sum of three exponentials with the FluoFit software (PicoQuant GmbH).

FTIR *spectroscopy:* FTIR spectra were acquired with a μ-FTIR spectrophotometer (LUMOS II, Bruker) in ATR mode. Measurements were carried out on the powders of pGO and dGO 12 deposited onto glass microscope slides, differently from the dy-w 12 and dy-w 3.5 samples, which were deposited from their concentrated water dispersions. Each spectrum was recorded in the 4000–500 cm^{-1} range with 96 scans and a spectral resolution of 4 cm^{-1}.

X-ray photoelectron spectroscopy (XPS): All samples were deposited onto H-terminated Si(100) surface. For pGO and dGO, a 50 μl drop-casting of their corresponding 0.06 mg ml^{-1} dispersions was carried out, while dy-w 12 and dy-w 3.5 samples were drop-casted from their concentrated water dispersions. XPS measurements were carried out using an Omicron Nanotechnology Multiprobe MXPS system using a monochromatic Al Kα ($h\nu = 1486.7$ eV) x-ray source (Omicron XM-1000, 14 kV and 16 mA) and an analyzer pass energy of 20 eV. A take-off angle of 21° with respect to the sample surface normal was adopted. The experimental spectra were curve-fitted using a Shirley function for the secondary electrons background and pseudo-Voigt (30% Lorentzian weight) functions for the elastic peaks, with position and full-width at half-maximum allowed to optimize within narrow limits. The oxygen content was determined through the $R_{O/C}$ ratio obtained after the curve-fitting of the C 1s region, by means of the following equation [45]:

$$R_{O/C} = \frac{A_{C-OH} + 1/2A_{C-O-C} + A_{C=O} + 2A_{COOH}}{A_{C=C} + A_{C-OH} + A_{C-O-C} + A_{C=O} + A_{COOH}} \quad (1)$$

where the terms A_x represent the OFG peak areas obtained by curve fitting.

This approach allowed to rule out any possible contributions in the oxygen content either deriving from contaminants or from the support material (Si).

Similarly, the relative amount of the different OFGs was determined through the area of the peaks within the curve-fitting envelope of the C 1s region, with an uncertainty of $\pm 10\%$, according to the following equation:

$$A\%_{OFG} = \frac{A_{C-OH}\, or\, \frac{1}{2}A_{C-O-C}\, or A_{C=O}\, or A_{COOH}}{A_{C=C} + A_{C-OH} + 1/2A_{C-O-C} + A_{C=O} + A_{COOH}} \times 100. \quad (2)$$

Electrochemical measurements: For the electrochemical characterization, 50 μl of 0.06 mg ml^{-1} GO-derived material dispersions were drop-casted onto freshly prepared H-terminated n-type Si(100) 1.5 cm × 1.5 cm wafers and let dry at room temperature. These surfaces were used as working electrodes in an electrochemical cell, where the electrode window area was roughly the same of the electroactive drop-casted GO deposit (0.3 cm^2). The electrolyte used was an aqueous 0.1 M phosphate (K_2HPO_4/KH_2PO_4) buffered saline (PBS) solution, with pH = 7.2, and the electrodes were an Ag/AgCl (sat., reference, $E = 0.198$ V *vs*. NHE, all potential values are referred to this electrode) and a platinum wire (counter electrode). The samples were reduced by means of cyclic voltammetry (CV) between open circuit potential (OCV, typically close to −0.4 V) and −1.50 V, with a potential scan rate of 20 mV s^{-1}. All electrochemical measurements were performed using a Bio-Logic SP-150 potentiostat/galvanostat driven by the Bio-Logic EC-Lab® software.

3. Results and discussion

3.1. AFM characterization

In order to determine the thickness of pGO deposits obtained following a well-consolidated procedure (see Experimental Section), AFM measurements were performed. The data collected in figure 1(a) are compatible with the presence of bilayers with a broad distribution of lateral sizes [14, 46]. After dialyzing the pGO samples for 72 h using a membrane with a cut-off of 12–14 kDa (dGO 12 samples) the AFM image (figure 1(b)) reveals the disappearance of the quasi-spherical nanoparticles present in the pGO samples. To isolate these CNPs, the corresponding dialysis water, denominated dy-w 12, enriched with species with MW <12–14 kDa was concentrated for 24 h (see Experimental Section). The resulting sample was analyzed by AFM (figure 1(c)) showing species with shape and lateral dimensions different from the layers of pGO and with a thickness of up to 20 nm.

Encouraged by these preliminary results, we investigated the presence of smaller nanoparticles. To this aim, the above procedure was repeated by using a dialysis membrane with a lower MW cut-off, namely 3.5–5 kDa; by concentrating the water coming from this dialysis the corresponding CNP sample, dy-w 3.5, was obtained. The comparison between the AFM images (upper panels of figures 2(a) and (b)) taken on the dy-w 3.5 and dy-w 12 samples reveals the presence of nanostructures with sizes of 2.6 ± 0.5 nm and 5 ± 1 nm, respectively. As expected, the statistical analysis reported in figure 2(b) for the dy-w 12 sample (lower panel) shows a broader size distribution due to the contribution of the smaller GO fragments successfully isolated via dialysis performed with a lower cut-off membrane (dy-w 3.5 sample, figure 2(a)—lower panel).

3.2. UV–Vis and fluorescence spectroscopy characterization

The UV–Vis spectrum recorded on an aqueous dispersion of pGO (figure 3(a), black line) shows the main absorption at 232 nm with a shoulder at 300 nm, respectively ascribable to π–π^* and n-π^* electron transitions, that is still present in the dGO 12 sample (figure 3(a), red line) [2, 39, 47, 48].

Conversely, the dialysis waters containing the low MW fractions (dy-w 12 and dy-w 3.5) display optical properties that

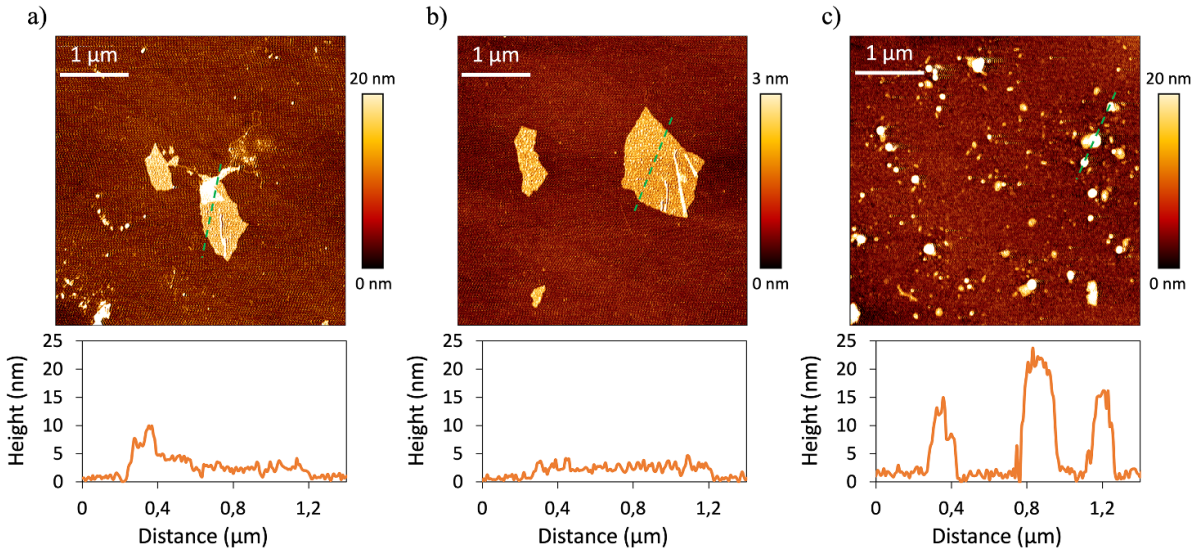

Figure 1. AFM tapping mode images of (a) pGO, (b) dGO 12, and (c) dy-w 12 samples with the respective height profiles tracked along the green dashed lines.

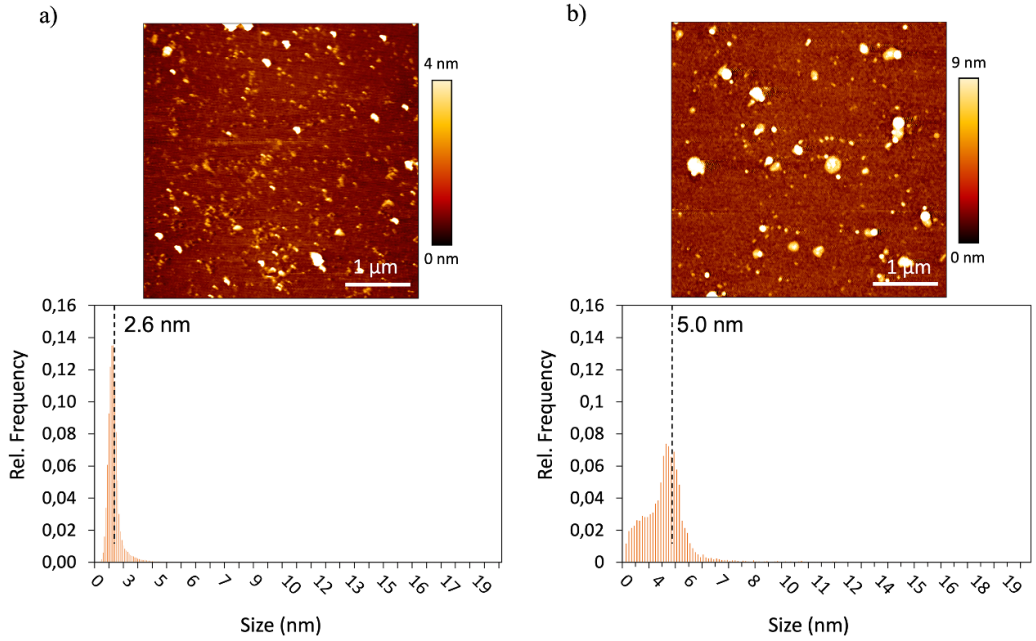

Figure 2. AFM-tapping mode images of (a) dy-w 3.5, and (b) dy-w 12 with the respective dimensional statistical analyses.

are significantly different from the layers of GO and dependent on the cut-off of the dialysis membranes used in the purification procedure (figure 3(b)). In particular, the main differences can be observed in the region below 400 nm, ascribable to the variation in the type and number of the carbon-based sp^2 domains and OFGs. In the dy-w 3.5 sample (figure 3(b), red line), a sharp absorption peak at 235 nm can be detected, suggesting that the aromatic C network is partially preserved in these low MW fragments. However, the UV–Vis spectra reported in figure 3(b), resemble those of amorphous CNPs (e.g. carbon nanodots) that typically display high optical absorption in the UV region of the electromagnetic spectrum [49–52].

In order to further characterize the samples obtained by the procedure proposed in this work, their relevant luminescence properties have been measured by exciting the samples at different wavelengths. The GO fluorescence is attributed to electron transitions between the non-oxidized carbon region and the boundary oxidized carbon atom region (C–O, C=O and carboxylate groups). As shown in figure 4, pGO and dGO 12 show a barely appreciable luminescence, with intensities sensibly lower than the corresponding water Raman scattering peak.

Correspondingly, as observed in figure 5, the concentrated waters obtained by the dialysis of GO (dy-w samples) show

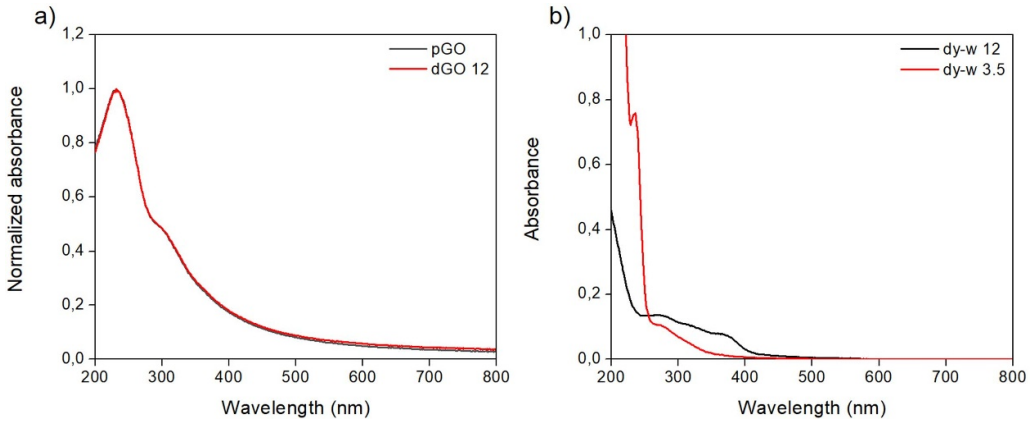

Figure 3. (a) Normalized UV–Vis spectra of pGO (black line) and dGO 12 (red line). (b) UV–Vis spectra of dy-w 12 (black line) and dy-w 3.5 (red line). All measurements were performed in water and at room temperature.

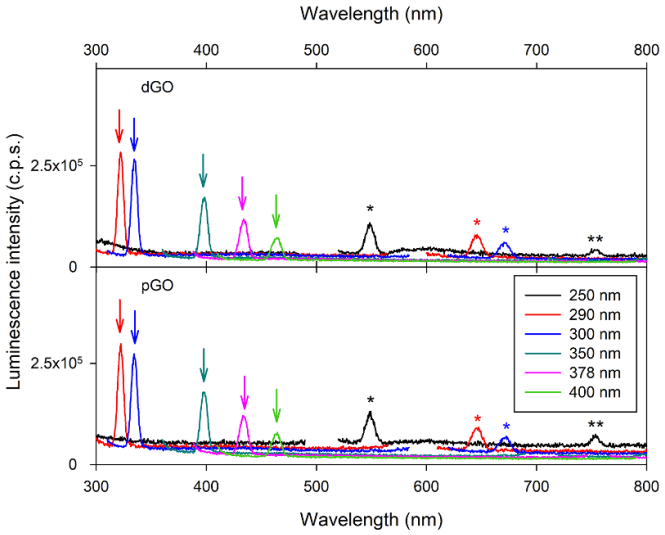

Figure 4. Emission spectra of pristine GO (pGO—lower panel) and dialyzed GO (dGO 12—upper panel) as a function of the excitation wavelength (see legend). Arrows indicate the relevant water Raman scattering peaks, while asterisks their respective 2nd and 3rd order Raman peaks.

a very high intensity of fluorescence emission compared to the GO-based samples, which suggests an increase in the amount of oxygenated functional groups, with their maxima that are function of the excitation wavelength (particularly for excitation wavelengths higher than 300 nm), as already documented in the literature [53]. Such an excitation wavelength dependence is attributed to the so-called red-edge-effect, a phenomenon bound to the solvation processes occurring during the lifetime of the electron excited state [54]. To describe the luminescence measured for GO derived materials, the determination of the decay profile of fluorescence signals is therefore recommended. In our case, it is interesting to note that the results obtained with pGO (figure S1—inset) are in very good agreement with those reported in the literature [55], considering the difference in the instrumental apparatus used. The GO decay in water at room temperature has been reported to be the sum of four exponential components, with lifetimes ranging from 30 ps to 1680 ps [55]. Since the electronics of the instrument used in this work is sensibly slower than that of the cited work, in our case the first three exponential components merged into one that accounted for more than 90% of the pGO decay, leaving an 8% of the decay described by an exponential component with a lifetime of 1.70 ns (figure S1—inset), in perfect agreement with the slower component found in the already cited [55].

To strengthen the fluorescence lifetime experiments, we performed an additional treatment of pGO with a dialysis membrane with a lower cut-off, 1.0 kDa, that also affords a sample with a luminescence dependent from the excitation wavelength (figure S2).

Compared to pGO (figure S1—inset) the luminescence lifetime of the concentrated dialysis water samples, dy-w 1.0, dy-w 3.5 and dy-w 12 (figure S1—main panel), is sensibly slower, therefore leading to an enhancement of the red-edge-effect on decreasing the dialysis membrane cut-off. As can be seen from figure S1, the differences among the three samples are truly modest. The fitting of the decays requires three exponential components, and the obtained lifetimes are in agreement with those found in the literature for GO sheets separated by centrifugation [56]. The corresponding lifetimes were indeed extremely close for the three different samples; therefore, the three decays have been globally fitted as the sum of three exponentials sharing the same time-decay constants (table S1). With this approach the fitting shown in the main panel of figure S1 (continuous red lines) were obtained, with random distributed residuals and χ^2 values close to unity (table S1).

Assigning these three components to specific fluorophores is beyond the scope of this work, assuming it was possible, given the complexity of the GO excited-state energy scenario [56]. One possible interpretative key could be to consider the origin of the different components as a consequence of the size heterogeneity of the CNPs present in the samples. If this were the case, it would be more correct to describe the kinetics of the decay process in terms of average kinetic constants (and, therefore, average lifetimes), each one characterized by a

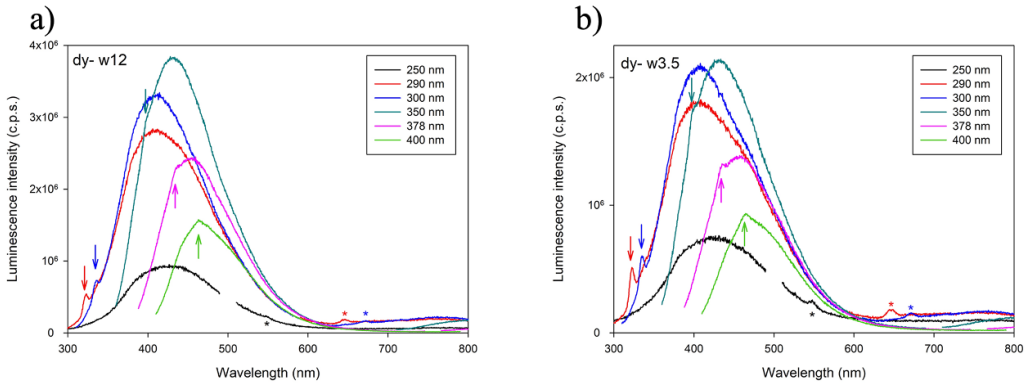

Figure 5. Excitation wavelength dependence (see legend) of the emission spectra of concentrated dialysis waters samples, (a) dy-w 12 and (b) dy-w 3.5. The colored arrows indicate, for each spectrum, the corresponding water Raman scattering peaks, with their 2nd order emissions barely visible for some excitation wavelengths (asterisks).

mean value with its relevant variance. From a practical point of view, this would correspond to fitting the data with a function that considers the mean lifetime value and the corresponding variance. Further work is necessary to address the correlation, if any, among the temporal profiles of the GO-derived CNP fluorescence and their dimensional polydispersity.

3.3. XPS characterization

XPS spectroscopy has disclosed the surface chemical composition of the GO-based and CNP materials. The efficiency of dialysis with respect to the basic purification steps, i.e. filtration and centrifugation, is evident in the comparison of the XPS survey spectra of the pGO and dGO 12 samples (figure S3). In fact, in the former spectrum the presence of impurities from the synthetic procedure is evident, i.e. sodium, sulfur, and nitrogen. These impurities almost disappear in dialyzed GO (dGO 12). The curve-fitted C 1s spectra of pGO and its purified derivatives, as well as the CNPs contained in the concentrated waters coming from the dialysis, are reported in figure 6. The C 1s spectrum of pGO (figure 6(a)) displays two main peaks, respectively ascribable to localized C sp^2 domains at 284.8 eV (red curve) and a convolution of C–O bonds from hydroxyl (286.4 eV, blue curve) and epoxide (287.0 eV, green curve) groups [57–59].

The peak tail at higher binding energy (BE) can be deconvoluted into two components, assigned to carbonyl/-carboxylate groups (288.1 eV, purple curve in figure 6(a)), and to the less abundant carboxyl moieties (289.2 eV, orange curve in figure 6(a)); the assignment of the various components to specific oxygenated functional groups has been supported by the theoretical work reported in the literature [59]. By using equation (1) (see Experimental Section), an O/C ratio ($R_{O/C}$) of 0.41 was calculated. Purification of pGO through dialysis with a 1.0 kDa cut-off membrane (dGO 1.0 sample, figure 6(b)) does not significantly affect the surface composition of the layers. In fact, the $R_{O/C}$ value remains constant (see table 1), probably due to the too low amount of removed tiny fragments.

When a higher cut-off (12–14 kDa) membrane is used for dialysis (dGO 12 sample, figure 6(c)), the removal of a higher amount of light fragments results in a slightly lower $R_{O/C}$ value (0.39), suggesting a partial loss of overoxidized GO layers as a consequence of the purification process. In particular, the relative concentration of hydroxyl groups calculated by using equation (2) (see Experimental Section) significantly decreases, passing from 17.2 to 15.6 and to 11.5%, along the sequence pGO, dGO 1.0, dGO 12 (see table 1).

Notably, the CNPs isolated by concentrating the dialysis waters (dy-w 12 and dy-w 3.5 samples, figures 6(d) and (e)) are especially rich in hydroxyl and carboxyl groups, at the expenses of epoxide moieties. In fact, compared to pGO, spectrum *d* of figure 6 (dy-w 12) displays a modified line shape, with a sizeable increase of the C–OH (286.3 eV, blue curve) and COOH (286.3 eV, orange curve) contributions paralleled by the decrease of the epoxy one, with percentage amounts of 33.4, 7.6 and 3.0%, respectively for C–OH, COOH and C–O–C. Consequently, the $R_{O/C}$ value rises up to 0.53 for the dy-w 12 sample, coherently with the expected higher oxygen content reported for the OD debated in the literature [23]. Finally, the dy-w 3.5 sample (figure 6(e)), constituted by fragments with MW $<$ 3.5 kDa, is characterized by the total suppression of epoxy functional groups, paralleled by intense C–OH (26.9%) and COOH (4.8%) contributions (see table 1), resulting in a $R_{O/C}$ value of 0.39.

Remarkably, the BE position of the C–OH component is found to decrease from 286.6 eV of pGO and dGO samples to 286.3 eV of the CNP dy-w samples. This shift is compatible with a variation in the nature of the GO C atoms bound to the—OH group, since the former BE position is more typical of basal C–OH groups (involving sp^3-C atoms), while the latter can be assigned to phenol-like groups at the edges of GO (with sp^2-C atoms) [59]. According to our XPS results, the

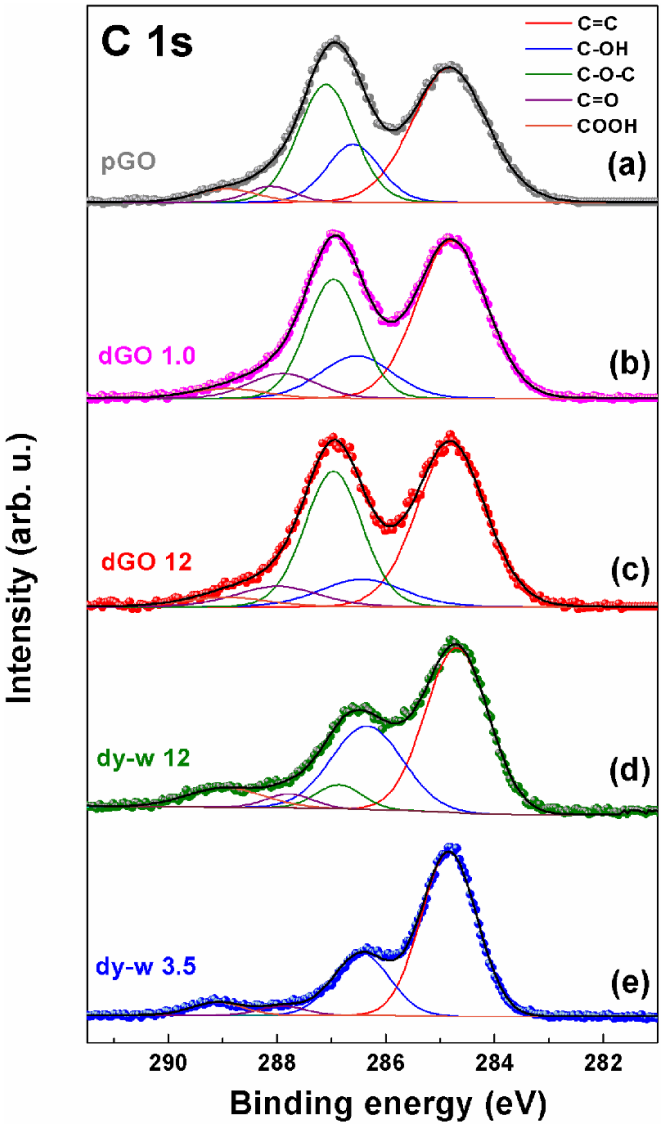

Figure 6. XPS spectra in the C 1s region of (a) pGO, (b) dGO 1.0, (c) dGO 12, (d) dy-w 12 and (e) dy-w 3.5. Experimental data are reported in dots, while curve-fitting results are reported with continuous colored lines, corresponding to different oxygenated functional groups (see legend).

Table 1. Percent amount[a] of relevant oxygenated functional groups in GO samples obtained from XPS C 1s spectra[b].

Sample	C=C	C–OH	C–O–C	C=O	COOH	$R_{O/C}$[c]
pGO	55.8	17.2	18.3	4.1	4.6	0.41
dGO 1.0	55.9	15.6	16.4	8.4	3.7	0.41
dGO 12	56.3	11.5	19.6	8.5	3.9	0.39
dy-w 12	53.2	33.4	3.0	2.8	7.6	0.53
dy-w 3.5	65.2	26.9	—	3.0	4.8	0.39

[a] Calculated according to equation (2), see Experimental Section.
[b] Associated error is ±10%.
[c] Calculated according to equation (1), see Experimental Section.

low MW GO fragments obtained with the mild approach here proposed, that may roughly correspond to the OD reported in the recent years in the literature, are constituted by layers with nearly unoxidized aromatic C basal planes whose edges are particularly rich in C–OH (phenols) and COOH (carboxyls) functional groups. Furthermore, the higher $R_{O/C}$ value found in the dy-w 12 sample compared to pGO, together with the general OFG enrichment at the edges of the layers for both dy-w samples is consistent with their enhanced luminescence properties.

3.4. Electrochemical characterization

In figure 7, the cyclic voltammograms (CV) corresponding to the samples investigated with XPS (see above) are reported, except for the case of the dy-w 1.0 sample, which was present in such a low amount that its current signal was hardly detectable. The CV profile of pGO (figure 7(a)) displays a series of reduction features that can be associated to epoxy (I), carbonyl (II) and basal hydroxyl (III) groups (see table 2 for their reduction potential values). Feature IV does not stem from a functional group of GO, but is more likely associated with water reduction adsorbed onto GO or intercalated within its layers, as we recently reported [59]. After feature IV, reduction of bulk water with continuous H_2 evolution is seen. Stepping to the dGO 1.0 sample (figure 7(b)), only small differences can be detected, since all the three features related to the OFGs in GO are found, while feature IV appears to decrease. This decrease turns out to be total in dGO 12 (figure 7(c)), where only features I, II and III can be detected, with the first two somewhat convoluted into a single broad component, and the third still quite intense.

Regarding the CV of the low MW sample dy-w 12 (figure 7(d)), we managed to obtain a fairly concentrated amount of it via drop-casting onto the Si electrode. Even though the detected current was much lower than the other samples (see the relevant current scale bars), the resulting voltammogram is still legible, displaying a single faint component in the region with the I and II features, and no signal from the component III.

Overall, the results from the electrochemical characterization via CV appear to match the outcome of XPS spectra. In fact, in pGO and dyalized GO samples little changes can be found related to OFGs. The most striking difference revealed by CV is the gradual disappearance of component IV from pGO to dGO 12 sample. Therefore, it is apparent that physisorbed and/or H-bound water molecules are more characteristic of the low MW fraction of GO, with which they interact more strongly, making these small fragments inherently highly hygroscopic, as actually visually experienced in this study. Since feature IV is anyway absent in the CV of dy-w 12 sample, we hypothesize that in pGO the small fragments are intercalated within the stacked layers of GO deposited onto the electrode, with the adsorbed water molecules behaving like electroactive functional groups of GO. On the other hand, when a CV is run on the isolated CNPs (dy-w 12 sample), the adsorbed water molecules are in direct contact with the bulk water and their electroactivity converges at more negative potentials to that of the hydrogen evolution reaction.

Furthermore, also the component III disappears in the dy-w 12 sample CV profile. According to XPS (see spectra in

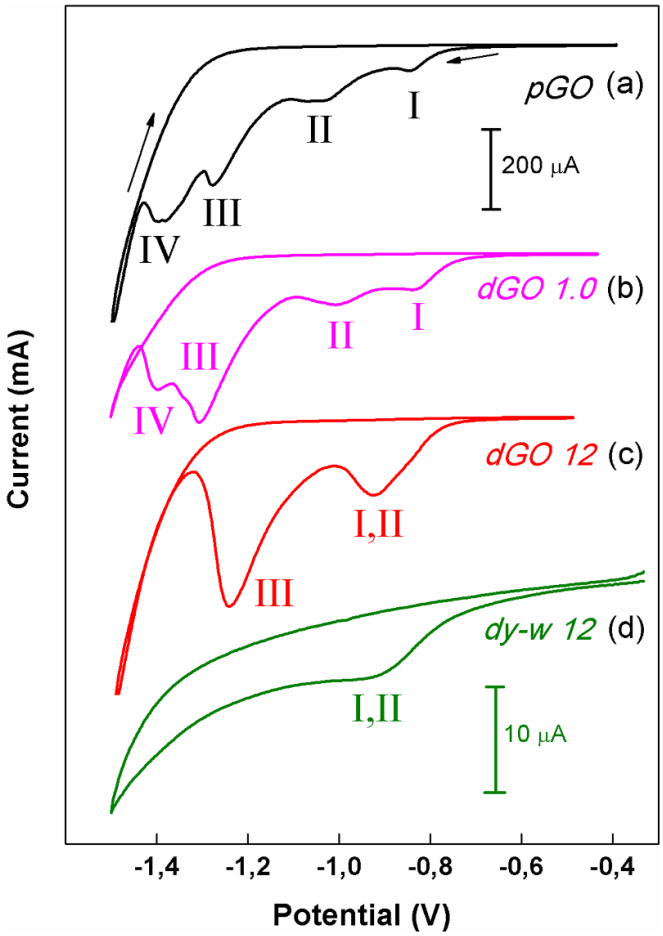

Figure 7. Cyclic voltammograms of (a) GO, (b) dGO 1.0, (c) dGO 12 and (d) dy-w 12 samples. Roman numerals indicate the relevant features discussed in the text. Measurements were run in 0.1 M PBS buffer solution (pH = 7.2) at a 20 mVs^{-1} potential scan rate. CVs in *a, b* and *c* panels are to scale (see black current scale bar), while CV in *d* panel is magnified for the sake of clarity (see green current scale bar).

Table 2. Reduction potential values (V) of the features resulting from cyclic voltammetry of the sample addressed in this work.

	I (epoxy)	II (carbonyl)	III (hydroxyl)[a]	IV (adsorbed water)
pGO	−0.84	−1.04	−1.27	−1.39
dGO 1.0	−0.83	−1.00	−1.30	−1.39
dGO 12		−0.92	−1.24	—
dy-w 12		−0.94	—	—

[a] sp^3-C in the GO basal plane.

figures 6(d) and (e)) the low MW fragments isolated by dialysis are rich in C–OH groups, but these are more compatible to phenol-like moieties confined to the edges of the GO layers. This finding is coherent with the CV trace reported in figure 7(d), since phenol C–OH groups are hardly electrochemically reducible, at least within the potential window explored [59]. Therefore, both XPS and CV techniques provide an unambiguous interpretation of the structure of the low MW CNPs: poorly oxidized aromatic C basal planes with edges particularly rich in phenolic and carboxylic functional groups (see figure 8 for a pictorial representation). The presence of OFGs in both GO-based samples and CNPs collected through dialysis is further supported by FT-IR spectroscopy (figures S4(a) and (b)), while the presence of graphitic areas and defects in the GO layers have been confirmed by Raman spectroscopy (figure S5).

4. Conclusions

To our knowledge, for the first time we have isolated and thoroughly characterized zero-dimensional nanoparticles obtained using a very mild approach for the purification of GO synthesized with the Hummers protocol. The proposed method is based on dialysis and has the outstanding advantage of avoiding any chemical process possibly affecting the composition of the GO layers, such as base washing. Consequently, through a multi-technique characterization approach, including AFM,

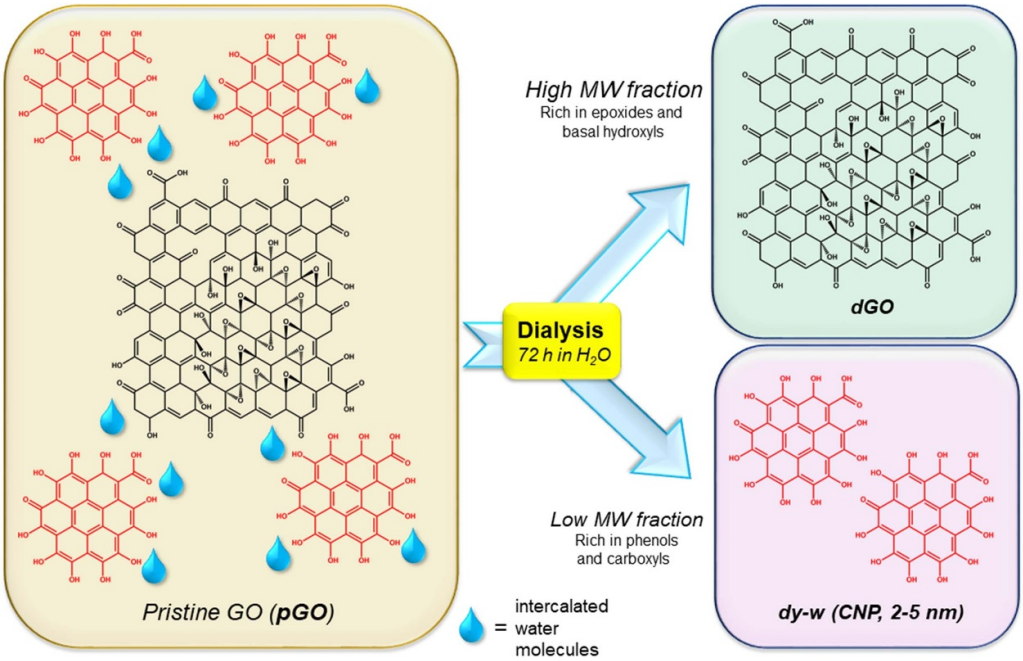

Figure 8. Pictorial representation of the isolation of the different GO components throughout the dialysis process. (Left) The pristine compound is characterized by the coexistence of large oxidized flakes and small edge-oxidized layers. In the solid pGO, these small layers are bound to large flakes via intercalated water molecules. (Right) after dialysis, the small layers are separated from the large flakes and in the solid state they tend to form CNPs, probably via π–π stacking and H–bonds, with lateral dimensions of 2–5 nm.

XPS, cyclic voltammetry and fluorescence spectroscopy, we have successfully demonstrated that the purified CNPs have dimensions in the 2–5 nm range and display an intense excitation-dependent fluorescence. They are constituted by GO layers, mostly oxidized at the edges with hydroxyl and carboxyl groups, which are likely stacked due to π–π interaction among their aromatic basal planes and H–bonded via their oxidized groups. In addition, we have shown that the solid-state pGO obtained from the Hummers synthesis is a composite material in which the CNPs are bound to the larger flakes through the presence of intercalated water molecules.

Purifying GO by dialysis consumes a moderate amount of water, but is easy and avoids the use of harmful chemicals. Furthermore, the dialysis procedure can be potentially scaled up to a medium laboratory scale.

Not only we do propose the dialysis method as an indispensable step towards more controlled and homogeneous GO samples, but also for the obtainment and potential valorization of GO luminescent nanoparticles. Indeed, dialyzed GO is expected to promote more reproducible functionalization processes due to a more homogeneous structure and a lower impact of competitive reactions. Furthermore, the separated CNPs could be turned into a high value side-product, in applications such as fluorescent sensing and imaging and sensitizers for solar cells. At the same time, the results here presented constitute a step forward in the comprehension of the GO structure at varying dimensions of its constituent layers.

Data availability statement

All data that support the findings of this study are included within the article (and any supplementary files).

Acknowledgments

F A acknowledges the ‘Avvio alla ricerca-2023’ Project funded by the Sapienza University of Rome (AR22318876732FE7). P A and F A acknowledge funding from the European Union—NextGenerationEU under the National Recovery and Resilience Plan (NRRP), Mission 4 Component 2 Investment 1.3—Call for tender No. 1561 of 11.10.2022 of Ministero dell’Università e della Ricerca (MUR), Project code PE0000021, CUP B53C22004070006, Project ‘Network 4 Energy Sustainable Transition—NEST’. M P and V P acknowledge funding from AIRC under IG 2019-ID. 23124 project, and from the Italian Ministry of Health, GR-2019-12370086. Use of FTIR equipment was possible

thanks to Sapienza University of Rome Grant for scientific equipment (2019, Protocol No. MA21916B755D01C9).

Conflict of interest

The authors declare that they have no known competing financial interests or personal relationships that could have appeared to influence the work reported in this paper.

ORCID iDs

Francesco Amato https://orcid.org/0000-0003-1577-7421
Leonardo Giaccari https://orcid.org/0009-0008-2620-9888
Sara Colecchia https://orcid.org/0009-0002-9648-9316
Valentina Palmieri https://orcid.org/0000-0002-6358-9647
Massimiliano Papi https://orcid.org/0000-0002-0029-1309
Pietro Altimari https://orcid.org/0000-0002-6638-1091
Alessandro Motta https://orcid.org/0000-0003-0235-2088
Mauro Giustini https://orcid.org/0000-0001-9390-0240
Robertino Zanoni https://orcid.org/0000-0003-2419-309X
Andrea Giacomo Marrani https://orcid.org/0000-0002-3203-9642

References

[1] Halbig C E, Mukherjee B, Eigler S and Garaj S 2024 *J. Am. Chem. Soc.* **146** 7431–8
[2] Guo S, Garaj S, Bianco A and Ménard-Moyon C 2022 *Nat. Rev. Phys.* **4** 247–62
[3] Lin H *et al* 2024 *ACS Nano* **18** 6038–94
[4] Wu J, Lin H, Moss D J, Loh K P and Jia B 2023 *Nat. Rev. Chem.* **7** 162–83
[5] Paulista Neto A J and Fileti E E 2018 *Phys. Chem. Chem. Phys.* **20** 9507–15
[6] Shao J J, Lv W and Yang Q H 2014 *Adv. Mater.* **26** 5586–612
[7] Wang X, Bai H and Shi G 2011 *J. Am. Chem. Soc.* **133** 6338–42
[8] Jerigová M, Odziomek M and López-Salas N 2022 *ACS Omega* **7** 11544–54
[9] Dimiev A, Kosynkin D V, Alemany L B, Chaguine P and Tour J M 2012 *J. Am. Chem. Soc.* **134** 2815–22
[10] Amato F *et al* 2023 *Adv. Mater. Interfaces* **10** 2300105
[11] Tiberio F *et al* 2024 *Mater. Adv.* **5** 4772–85
[12] Palmieri V *et al* 2018 *2D Mater.* **5** 015027
[13] Chen J, Zhang Y, Zhang M, Yao B, Li Y, Huang L, Li C and Shi G 2016 *Chem. Sci.* **7** 1874–81
[14] Amato F, Motta A, Giaccari L, Di Pasquale R, Scaramuzzo F A, Zanoni R and Marrani A G 2023 *Nanoscale Adv.* **5** 893–906
[15] Brisebois P P and Siaj M 2020 *J. Mater. Chem.* C **8** 1517–47
[16] Krishnamoorthy K, Veerapandian M, Yun K and Kim S J 2013 *Carbon* **53** 38–49
[17] Gurzęda B, Boulanger N, Jørgensen M R V, Kantor I and Talyzin A V 2024 *Carbon* **221** 118899
[18] Cai M, Thorpe D, Adamson D H and Schniepp H C 2012 *J. Mater. Chem.* **22** 24992–5002
[19] Eigler S and Hirsch A 2014 *Angew. Chem., Int. Ed.* **53** 7720–38
[20] Dimiev A M and Tour J M 2014 *ACS Nano* **8** 3060–8
[21] Zhang L, Liang J, Huang Y, Ma Y, Wang Y and Chen Y 2009 *Carbon* **47** 3365–8
[22] Rourke J P, Pandey P A, Moore J J, Bates M, Kinloch I A, Young R J and Wilson N R 2011 *Angew. Chem., Int. Ed.* **50** 3173–7
[23] de Lima A H, Scarpa I, Azevedo N C L, Lelis G C, Strauss M, Martinez D S T and Furlan de Oliveira R 2023 *J. Mater. Chem.* C **11** 12429–52
[24] Rodriguez-Pastor I, Ramos-Fernandez G, Varela-Rizo H, Terrones M and Martin-Gullon I 2015 *Carbon* **84** 299–309
[25] Bonanni A, Ambrosi A, Chua C K and Pumera M 2014 *ACS Nano* **8** 4197–204
[26] Thomas H R, Vallés C, Young R J, Kinloch I A, Wilson N R and Rourke J P 2013 *J. Mater. Chem.* C **1** 338–42
[27] Li W, Tang H, Zhang D, Huang T and Xing B 2024 *Environ. Sci. Technol.* **58** 5963–73
[28] Thomas H R, Day S P, Woodruff W E, Vallés C, Young R J, Kinloch I A, Morley G W, Hanna J V, Wilson N R and Rourke J P 2013 *Chem. Mater.* **25** 3580–8
[29] Hu C, Liu Y, Yang Y, Cui J, Huang Z, Wang Y, Yang L, Wang H, Xiao Y and Rong J 2013 *J. Mater. Chem.* B **1** 39–42
[30] Tang T, Liu F, Liu Y, Li X, Xu Q, Feng Q, Tang N and Du Y 2014 *Appl. Phys. Lett.* **104** 123104
[31] Faria A F, Perreault F and Elimelech M 2018 *ACS Appl. Nano Mater.* **1** 1164–74
[32] Guo Z, Wang S, Wang G, Niu Z, Yang J and Wu W 2014 *Carbon* **76** 203–11
[33] Dimiev A M and Polson T A 2015 *Carbon* **93** 544–54
[34] Fan X, Peng W, Li Y, Li X, Wang S, Zhang G and Zhang F 2008 *Adv. Mater.* **20** 4490–3
[35] Dimiev A M, Alemany L B and Tour J M 2013 *ACS Nano* **7** 576–88
[36] Panigrahi P K, Chandu B and Puvvada N 2024 *ACS Omega* **9** 3092–122
[37] Yang Z, Xu T, Li H, She M, Chen J, Wang Z, Zhang S and Li J 2023 *Chem. Rev.* **123** 11047–136
[38] Ferguson V, Silva S R P and Zhang W 2019 *Energy Environ. Mater.* **2** 107–18
[39] Marcano D C, Kosynkin D V, Berlin J M, Sinitskii A, Sun Z, Slesarev A, Alemany L B, Lu W and Tour J M 2010 *ACS Nano* **4** 4806–14
[40] Chen J, Li Y, Huang L, Li C and Shi G 2015 *Carbon* **81** 826–34
[41] Amato F, Ferrari I, Motta A, Zanoni R, Dalchiele E A and Marrani A G 2023 *RSC Adv.* **13** 29308
[42] Liscio A, Kouroupis-Agalou K, Betriu X D, Kovtun A, Treossi E, Pugno N M, De Luca G, Giorgini L and Palermo V 2017 *2D Mater.* **4** 025017
[43] Airoldi M, Barone G, Gennaro G, Giuliani A M and Giustini M 2014 *Biochem* **53** 2197–207
[44] Tasca E, Del Giudice A, Galantini L, Schillén K, Giuliani A M and Giustini M 2019 *J. Colloid Interface Sci.* **540** 593–601
[45] Marrani A G, Coico A C, Giacco D, Zanoni R, Scaramuzzo F A, Schrebler R, Dini D, Bonomo M and Dalchiele E A 2018 *Appl. Surf. Sci.* **445** 404–14
[46] Jalili R, Aboutalebi S H, Esrafilzadeh D, Konstantinov K, Moulton S E, Razal J M and Wallace G G 2013 *ACS Nano* **7** 3981–90
[47] Palmieri V, Dalchiele E A, Perini G, Motta A, De Spirito M, Zanoni R, Marrani A G and Papi M 2019 *Chem. Commun.* **55** 4186–9
[48] Otsuka H, Urita K, Honma N, Kimuro T, Amako Y, Kukobat R, Bandosz T J, Ukai J, Moriguchi I and Kaneko K 2024 *Nat. Commun.* **15** 1708
[49] Martindale B C M, Hutton G A M, Caputo C A and Reisner E 2015 *J. Am. Chem. Soc.* **137** 6018–25
[50] Martindale B C M, Hutton G A M, Caputo C A, Prantl S, Godin R, Durrant J R and Reisner E 2017 *Angew. Chem.* **129** 6559–63

[51] Amato F, Soares M C P, Cabral T D, Fujiwara E, Cordeiro C M D B, Criado A, Prato M and Bartoli J R 2021 *ACS Appl. Nano Mater.* **4** 9738–51
[52] Filippini G, Amato F, Rosso C, Ragazzon G, Vega-Peñaloza A, Companyó X, Dell'Amico L, Bonchio M and Prato M 2020 *Chem* **6** 3022–37
[53] Cushing S K, Li M, Huang F and Wu N 2014 *ACS Nano* **8** 1002–13
[54] Xiao X, Zhang Y, Zhou L, Li B and Gu L 2022 *Nanomaterials* **12** 2444
[55] Shang J, Ma L, Li J, Ai W, Yu T and Gurzadyan G G 2012 *Sci. Rep.* **2** 792
[56] Zhang X F, Shao X and Liu S 2012 *J. Phys. Chem.* A **116** 7308–13
[57] Lin C Y, Cheng C E, Wang S, Shiu H W, Chang L Y, Chen C H, Lin T W, Chang C S and Sen Chien F S 2015 *J. Phys. Chem.* C **119** 12910–5
[58] Larciprete R, Lacovig P, Gardonio S, Baraldi A and Lizzit S 2012 *J. Phys. Chem.* C **116** 9900–8
[59] Ferrari I, Motta A, Zanoni R, Scaramuzzo F A, Amato F, Dalchiele E A and Marrani A G 2023 *Carbon* **203** 29–38